ACS OMEGA

Open Access

http://pubs.acs.org/journal/acsodf

Article

Designing Porosity-Tailored Hydrogel Sponges with Controlled Cell Positioning Using Dispersible, Autofragmented Sacrificial Microfibers

Aruto Hori, Mizuki Hirata, Rina Nonogaki, Rie Utoh, and Masumi Yamada*

Cite This: *ACS Omega* 2025, 10, 11900−11910

Read Online

ACCESS | Metrics & More | Article Recommendations | Supporting Information

ABSTRACT: Hydrogel encapsulation is a rational approach that facilitates three-dimensional inoculation, arrangement, and culture of living mammalian cells for biomedical applications. However, strategies to form capillary-like conduits in hydrogels remain challenging due to low spatial resolution and difficulty in controlling the location of multiple cell types. Herein, we propose a highly unique process of constructing hydrogel sponges with tailored pore densities using finely fragmented microfibers as sacrificial porogens. A facile production process for automatically fragmented hydrogel microfibers (AF fibers) was developed through micronozzle-assisted hydrodynamic spinning and shear force application during gelation. Hydrogel sponges were prepared using photo-cross-linkable gelatin as the matrix and AF fibers dispersed in the precursor solution. We cultured liver cells in the sponges and evaluated the morphology and pore connectivity of the sponges and cellular functions. Furthermore, to create tissue models highly mimicking the cellular assembly *in vivo*, coculture of two types of cells was demonstrated in a position-controlled manner using cell-encapsulating AF fibers. The proposed approach of rationally designing hydrogel sponges is highly versatile in 3D cell culture for cell-based drug evaluation and regenerative medicine because of the simplicity of preparation and its impact on cellular functions.

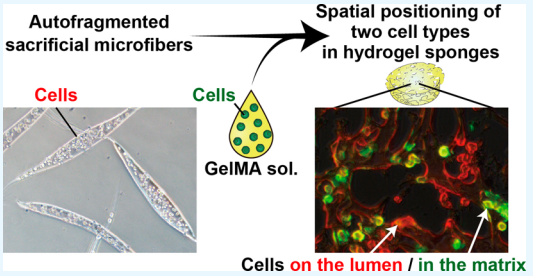

1. INTRODUCTION

Three-dimensional (3D) mimicry of living tissues with appropriate cellular microenvironments offers alternatives to cell-based drug evaluation and regenerative therapies. In particular, tailoring the matrix properties while considering physiological cell−cell interactions allows for the accurate reproduction of organ-associated cellular functions.[1] Innovations in additive manufacturing and 3D bioprinting technologies have opened new ways to create tissue equivalents by finely assembling multiple cells.[2] Many approaches for the rational design of hydrogel-based 3D cell culture systems have been presented using alginate,[3] PEGDA,[4] and photo-cross-linkable gelatin-based precursor solutions[5,6] as cell-supportive matrices. Additionally, more advanced functionalities of tissue models have been realized by coculturing heterotypic cells,[7−9] chemically functionalizing biopolymers,[10,11] and tuning the mechanical properties of hydrogels.[12−14]

When cells are embedded in hydrogels at a high density, similar to *in vivo* tissues, the supply of nutrients and oxygen to the cells located deep within the hydrogel does not meet the standards required by the cells. The microenvironment for cells positioning near the center of multicellular spheroids becomes hypoxic when the spheroid size becomes larger than approximately 200 μm.[15−18] This situation is similar for hydrogel-based cell culture systems; O_2 levels within the hydrogel matrix rapidly decrease, and cell necrosis occurs in areas distant from the surface.[19,20]

Therefore, attempts have been made to create vascular network-like conduits in tissue constructs. Researchers have proposed unique approaches for preparing hydrogels with embedded interconnected micropores. A representative example is the 3D bioprinting method using two types of bioinks: one forming a cell-embedded hydrogel matrix, and the other forming pores as a sacrificial support material.[21,22] Based on this process, vasculature network-like structures were fabricated using an alginate hydrogel or fugitive Pluronic F-127 ink as a sacrificial material.[23,24] Techniques for the accumulation and assembly of cell-adhesive microbeads have also been developed to form 3D tissues with internal pores;[25−27] the spaces between the beads function as densely arranged conduits, thus solving the problem of relatively low resolution in 3D bioprinting techniques. Additionally, unique phase-separation behaviors of aqueous polymer solutions have

Received: September 17, 2024
Revised: January 23, 2025
Accepted: January 30, 2025
Published: February 10, 2025

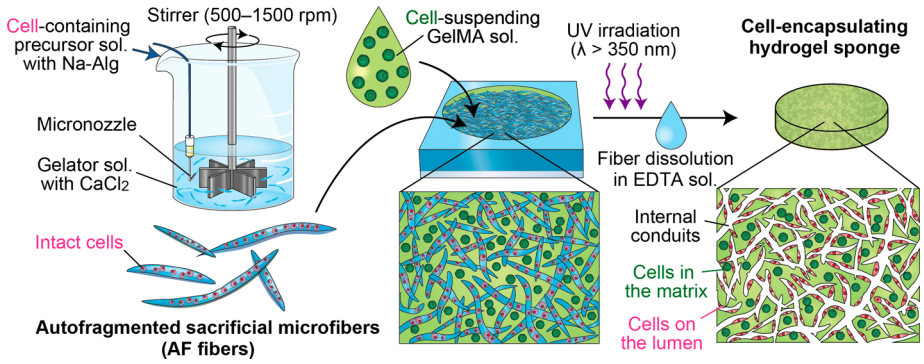

Figure 1. Schematic showing the concept of this study. Autofragmented sacrificial microfibers (AF fibers) were prepared by shear-assisted hydrodynamic spinning, and then they were used as sacrificial porogens to create cell-encapsulating hydrogel sponges with internal conduits. Coculture of two types of cells at different positions (in the hydrogel matrix and on the lumen) is achieved.

recently been applied to the formation of hydrogel sponges.[28−30]

Among various technologies to form capillary structures, the use of microfibers or microbeads as sacrificial porogens is a promising method.[22,31] Such micrometer-sized materials as sacrificial porogens allow for the precise control of pore morphology and density, as well as the creation of capillary-sized conduits with high precision. Moreover, introduction of cells into the inner surface of the lumen is possible using sacrificial materials with embedded living cells.[32,33] Microbeads are the most commonly used porogens because they are easy to fabricate; however, the morphology of the lumen formed by spherical beads is completely different from that of vascular networks in living tissues. Furthermore, porosity cannot be widely tailored because the volume ratio of the beads must be sufficiently high to ensure pore connectivity. Microfibers as an alternative material may be advantageous in terms of the formation of linear conduits; however, complicated protocols and devices are required to produce such fibers.[34,35] In addition, to disperse the fibers uniformly in precursor solutions for preparing hydrogels, a fragmentation process mostly involving manual cutting operation is required.

To overcome these limitations, a new strategy is required to efficiently produce fragmented fiber-type porogens without any complicated and labor-intensive protocols. Ideally, such a material should be (i) dispersible in an aqueous solution of a hydrogel precursor solution without entanglement, (ii) amenable to encapsulating intact cells, (iii) easily removable or dissolvable, and (iv) controllable in the morphology, especially the fragmentation length. To the best of our knowledge, methods for efficiently preparing hydrogel microfibers that are fragmented into desired lengths without mechanical cutting processes and are capable of encapsulating intact cells in the matrix have not been established. Hydrogel sponges prepared using fiber-type porogens are advantageous because interconnected pores are easily formed, and their size and density are tunable. The morphological similarity of such hydrogel sponges to tissue microenvironments *in vivo* would upregulate cellular functions in *in vitro* culture platforms.

In the present study, we developed a new method for efficiently producing sacrificial, autofragmented, and fiber-type porogens that can be utilized for creating hydrogel sponges. As shown in Figure 1, a micronozzle-based hydrodynamic spinning process for Ca-alginate hydrogel fibers with a combination of shear force applications is proposed. The resulting autofragmented microfibers (AF fibers) were then used as high-density porogens to create a hydrogel sponge with a tailored internal pore density. We used GelMA as a matrix for the hydrogel sponge, cultured liver cells (HepG2 cells) in the hydrogel matrix, and characterized their viability, proliferation, and function. In addition, we demonstrated the position control of the two cell types by coculturing them inside the hydrogel matrix and on the lumen of the pores.

2. MATERIALS AND METHODS

2.1. Preparation of GelMA. GelMA was prepared according to previously established protocols[28,36] with minor modifications. In brief, gelatin (type A, from porcine skin, Sigma-Aldrich, MO, USA) was dissolved in phosphate buffered saline (PBS) at 50 °C at a concentration of 10% (w/v). Methacrylic anhydride (final conc. of 7% (v/v), Sigma-Aldrich) was added to this solution, and the mixture was stirred for 2 h at 50 °C to proceed the methacrylation reaction. The mixture was dialyzed in DI water using a dialysis membrane (size 36; Fujifilm Wako Pure Chemical, Osaka, Japan) for 7 days. The purified GelMA solution was freeze-dried using a freeze-dryer (FDS-1000, EYELA, Tokyo, Japan) to obtain the dried GelMA powder, which was stored at −20 °C until use.

2.2. Cell Culture and Preparation. HepG2 (human hepatoma cell line) and Swiss 3T3 (mouse fibroblast cell line) cells were provided by Riken BRC (Ibaraki, Japan). These cells were cultured in DMEM (Fujifilm Wako) supplemented with 10% fetal bovine serum (Thermo Fisher Scientific, MA, USA), 100 U/mL penicillin, and 0.1 mg/mL streptomycin (Sigma-Aldrich) at 37 °C with 5% CO_2 in a CO_2 incubator. Cells at 70−80% confluency were harvested from cell culture dishes by trypsin−EDTA (Sigma-Aldrich) treatment. The harvested cells were suspended in saline and then large cell aggregates were removed using a cell strainer (mesh size of 70 μm, Corning, NY, USA). When coculturing HepG2 and Swiss 3T3 cells in the hydrogel sponge, these cells were stained green and red using PKH67 Green and PKH26 Red Fluorescent Cell Linker Kits (Sigma-Aldrich), respectively.

2.3. Preparation of Autofragmented Microfibers. The powder of sodium alginate (Na-Alg, high mannuronic acid content, IL-6M, KIMICA, Tokyo, Japan) was preheated at 100 °C for 10 min in a convection oven to reduce the possibility of microbial contamination. To prepare autofragmented microfibers (AF fibers) without encapsulating cells, an aqueous solution of 2.5% Na-Alg in saline was used as the precursor solution. A gelator solution (volume of 100 mL), which was an

https://doi.org/10.1021/acsomega.4c08536
ACS Omega 2025, 10, 11900−11910

aqueous solution of 20 mM $CaCl_2$, 0.72% NaCl, and 2% PEG (average Mw of 300,000−500,000, Fujifilm Wako), was stirred in a 300 mL beaker using a tornado stirrer (PM-201, AS ONE, Osaka, Japan). The precursor solution was continuously pumped into the stirred gelator solution using a syringe pump (KDS200, KD Scientific, MA, USA) through a Teflon tubing and a thin blunt-tip syringe needle (Ophthalmic Needle 30 G, Nipro, Osaka, Japan). The needle tip was bent 90° such that the extruded flow of the precursor solution was parallel to the surrounding flow (Figure 1). The generated AF fibers were washed with an aqueous solution of 20 mM $CaCl_2$ and 0.72% NaCl twice via gentle centrifugation. From microscopic images, the widths of the fibers were measured at three locations, and the average of these values was used as the diameter; at least 50 fibers were measured for each condition.

For preparing AF fibers encapsulating microparticles, 3.2 μm red fluorescent particles (R0300, Thermo Fisher Scientific) were suspended in the precursor solution at a concentration of approximately 5×10^7 particles/mL. To prepare Swiss 3T3 cell-encapsulating AF fibers, bovine serum albumin (BSA; final conc. of 0.5% (w/v); Rockland Immunochemicals, PA, USA) and HEPES (final conc. of 10 mM, Thermo Fisher Scientific) was added to the precursor solution. Swiss 3T3 cells were then added to this solution at a final conc. of 2.5×10^7 cells/mL and gently though thoroughly dispersed. Finally, AF fibers were prepared in the same way as described above.

2.4. Preparation of Hydrogel Sponges. First, the hydrogel sponges without embedding cells were prepared. Fibers encapsulating red fluorescent microparticles were used to evaluate the solubility of the AF fibers; otherwise, fibers without particles were employed. The suspension of the AF fibers was centrifuged, the supernatant was removed by pipetting and the remaining water was completely removed using a clean wipe. The fiber pellet was introduced into a chamber prepared by bonding a 1 mm thick silicone sheet with an 8 mm diameter hole and a flat glass slide. A photoinitiator (Irgacure 2959, BASF Japan, Tokyo, Japan) was added at a final concentration of 0.5% to a 30% GelMA solution containing 0.9% NaCl. This solution, warmed at 37 °C, was poured onto the pellet of the AF fibers in the chamber, with adjusting the volume of the fiber pellet and the GelMA solution by weighing. After gently and thoroughly mixing the suspension with tweezers, GelMA in this precursor solution was cross-linked by UV irradiation for 30 s each from the top and bottom surfaces using a UV irradiation system with a mercury lamp (UIV270, Ushio, Tokyo, Japan). Simultaneously, the UV light shorter than 350 nm was cut by a long-pass filter (ZUL0350, Asahi Spectra, Tokyo, Japan). The obtained hydrogel was collected from the chamber and placed in an aqueous solution of 75 mM EDTA-3Na at room temperature and gently shaken (72 rpm) for 45 min using a reciprocating shaker to dissolve the sacrificial AF fibers.

A similar procedure was used to prepare hydrogel sponges encapsulating living cells. The GelMA solution was premixed with a pellet of HepG2 cells at a final concentration of 2.5×10^7 cells/mL, and then, AF fibers were added to this solution and hydrogel sponges were prepared. For coculturing HepG2 cells and Swiss 3T3 cells, AF fibers encapsulating Swiss 3T3 cells were used. The obtained hydrogel sponges were placed in 60 mm dishes containing 7 mL of cell culture medium and incubated in a 5% CO_2 incubator. The culture medium was changed every 2 days.

2.5. Characterization of the Hydrogel Sponges. To observe the cross-sectional morphology of the hydrogel sponge, the hydrogel was embedded in O.C.T. compound (Sakura Finetek, Tokyo, Japan), frozen, and then thin sections (10 μm thick) were prepared using a cryostat (CM-1510S, Leika Microsystems, Eisfeld, Germany). The GelMA hydrogel matrix was stained with picrosirius red (Picrosirius Red Stain Kit, Polysciences, PA, USA) and observed under a phase-contrast/fluorescence microscope (IX71, Olympus, Tokyo, Japan).

The continuity of the pores in the hydrogel sponge was evaluated by two approaches. In the first method, AF fibers encapsulating the red 3.2 μm fluorescent microparticles were used, and the ratio of particles eluted from the GelMA hydrogel into the surrounding EDTA solution during fiber dissolution was evaluated. In the second method, an aliquot of a suspension of the red 3.2 μm and green 9.9 μm (G1000, Thermo Fisher Scientific) microparticles was dropped onto a hydrogel sponge, which was prepared using AF fibers without encapsulating particles and placed on a wipe. Thin frozen sections were prepared using the protocol described above and the positions of the particles in the cross sections were observed using the microscope.

2.6. Characterization of Cells in the Hydrogel Sponges. *2.6.1. Cell Viability Assay.* Live/Dead assay was performed for the HepG2 cells cultured in the hydrogel sponge at Days 0 and 3. The hydrogel sponge was cut into half in a vertical direction using a razor blade, and cells on the cross-section were stained using a Live/Dead Viability Kit (Thermo Fisher Scientific), according to the manufacturer's protocol.

2.6.2. Immunohistochemical Analysis of Ki-67. To characterize the proliferative ability of the encapsulated cells, the expression of Ki-67, a nuclear protein used as a proliferation marker, was investigated immunohistochemically. First, hydrogel sponges embedding cells were fixed overnight in 10% formalin neutral buffer solution (Fujifilm Wako), then dehydrated by ethanol, and embedded in paraffin. Thin sections with a thickness of 7 μm were prepared using a microtome (RX-860, Yamato Kohki, Saitama, Japan). For antigen retrieval, the dewaxed paraffin sections were autoclaved in citrate buffer (PH 6.0) at 121 °C for 7 min. The sections were blocked with 10% donkey serum, incubated with rabbit anti-Ki-67 antibody (ab15580; Abcam, Cambridge, UK), and then with donkey antirabbit IgG Alexa 594 (Thermo Fisher Scientific). Finally, the sections were mounted in ProLong gold antifade reagent with DAPI (Thermo Fisher Scientific) and observed using the microscope. The ratios of the Ki-67-positive cells were evaluated from approximately 300 cells for each sample in randomly selected images (n = 4) for both surface (<200 μm from the surface) and central regions (>200 μm from the surface) of the hydrogel.

2.6.3. Gene Expression Assay. The expressions of liver cell-specific genes of the HepG2 cells cultured in the hydrogel sponges were investigated using quantitative reverse transcription PCR (RT-qPCR). In the single culture condition, total RNA was extracted and purified from the cell-encapsulating hydrogel sponges at Days 4 and 7 using TRIzol reagent (Thermo Fisher Scientific) and a polytron homogenizer (PT 10/35, Kinematica AG, Malters, Switzerland). Then, a Pure Link RNA mini kit (Thermo Fisher Scientific). Genomic DNA was removed using DNase I (Thermo Fisher Scientific). Complementary DNA was synthesized from 0.2 μg of the template RNA using SuperScript IV VILO reverse

https://doi.org/10.1021/acsomega.4c08536
ACS Omega 2025, 10, 11900−11910

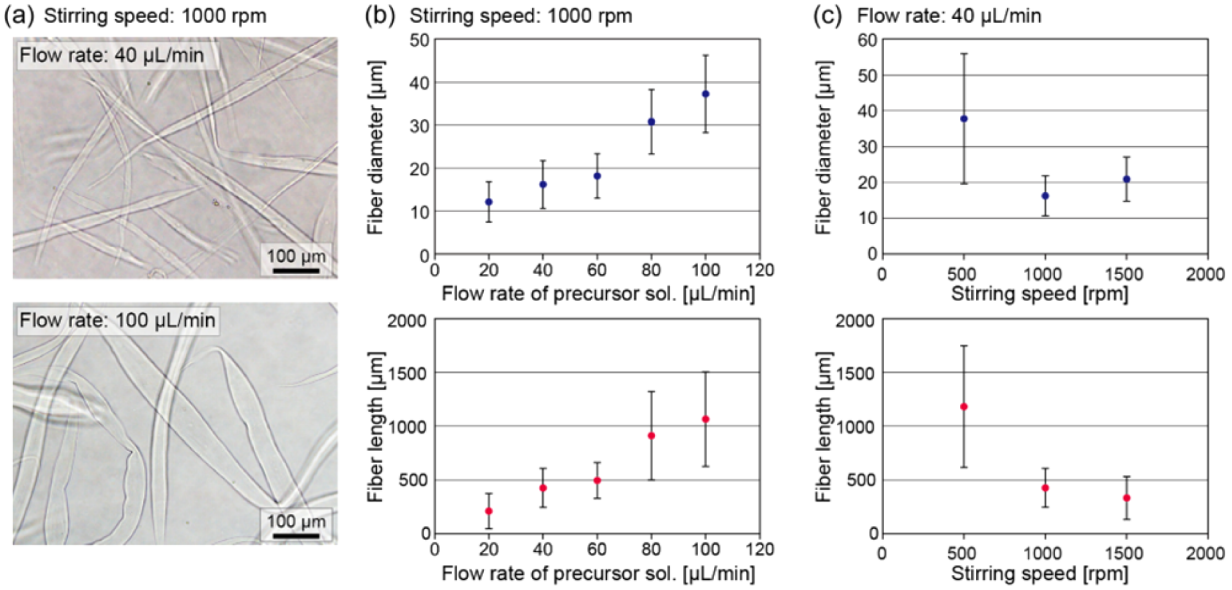

Figure 2. (a) Micrographs showing the AF fibers prepared under different conditions of the flow rate of the precursor solution. The stirring speed was 1000 rpm. (b, c) Effects of (b) the flow rate of the precursor solution and (c) the stirring speed on the diameter and length of the AF fibers. Each data shows the mean ± SD of at least 50 fibers.

transcriptase (Thermo Fisher Scientific). RT-qPCR analysis was performed with TaqMan Master Mix using the StepOnePlus Real-Time PCR System (Thermo Fisher Scientific). The expression levels of target and reference genes were evaluated using TaqMan probes and primers for albumin (*ALB*, Hs00609410_m1), ornithine transcarbamylase (*OTC*, Hs00166892_m1), apolipoprotein A1 (*ApoA1*, Hs00985000_g1), and hypoxanthine phosphoribosyltransferase 1 (*HPRT1*, Hs02800695_m1). Relative gene expression levels were analyzed using comparative CT method and normalized to the expression levels of *HPRT1* as the housekeeping control. Finally, the gene expression of the control 2D culture on a culture plate at Day 3 was normalized to 1. Gene expression analysis for the coculture condition was conducted similarly, using *GAPDH* (Hs99999905_m1) as the housekeeping control. The specificity of the TaqMan probes and primers for human cells (HepG2) was experimentally confirmed.

2.7. Statistical Analysis. The obtained data were statistically analyzed by *t*-test or one-way analysis of variance (ANOVA) with Games-Howell or Bonferroni *post hoc* tests using IBM SPSS Statistics software (IBM Japan, Tokyo, Japan). Differences were considered significant at $*p < 0.05$ and $**p < 0.01$.

3. RESULTS AND DISCUSSION

3.1. Preparation of Autofragmented Alginate Microfibers. There are several major requirements for fibers made of alginate hydrogel to be used as an efficient sacrificial material. First, the fiber diameter should be sufficiently small to form capillary-sized conduits. Second, the fibers must be fragmented into appropriate lengths and must be easily dissolved and removed. Several methods using microfluidic devices have been reported to produce alginate hydrogel microfibers. However, fragmented fibers can only be obtained by implementing complex physical cutting mechanisms,[37,38] or bubble-triggered fragmentation.[39,40] Therefore, in this study, we developed a new and efficient process to fabricate fibers that satisfy the aforementioned requirements. As shown in Figure 1, micronozzle-based hydrodynamic spinning combined with shear-induced fragmentation is proposed. Here high molecular weight PEG (Mw of 300,000−500,000) was added to the gelator solution to increase the shear force generated by stirring; the viscosity of the gelator solution was measured to be 20.5 mPa s at 25 °C.

Figure 2a shows microscopic images of the AF fibers obtained under different conditions together with the results of controlling the fiber morphology. When the flow rate of the Na-Alg solution was 40 μL/min and the stirring speed was 1000 rpm, the mean diameter of the obtained fibers was approximately 16 μm. Notably, the fibers were effectively fragmented with a mean length of 400−500 μm. The fiber ends were thin and sharp, probably because they were stretched by the shear forces generated by stirring during gelation. Under conditions without stirring, long fibers were formed and they were not fragmented (data not shown). Despite the use of a relatively large 30 G syringe needle as the micronozzle (OD: 300 μm; ID: 140 μm), fibers with much smaller diameters were obtained. This can be attributed to the dehydration of the precursor solution during gelation and the flow-focusing effect by the surrounding flow. To the best of our knowledge, no previous reports are available on the automatic fragmentation of micrometer-thick alginate fibers using a simple experimental setup. As the fibers were not too long, they were dispersed in the gelator solution without entanglement.

3.2. Morphology Control of the AF Fibers. Controlling the morphology of the AF fibers is of great importance for reducing entanglement and generating a network of conduits with the desired size and density in the hydrogel. Therefore, we attempted to control the length and diameter of the fibers by varying two factors that could crucially affect these parameters: the flow rate of the precursor solution and the stirring speed.

First, the flow rate of the precursor solution was varied. As shown in Figure 2b, the fiber diameter increased as the flow rate increased. Theoretically, if the flow velocity around the

https://doi.org/10.1021/acsomega.4c08536
ACS Omega 2025, 10, 11900−11910

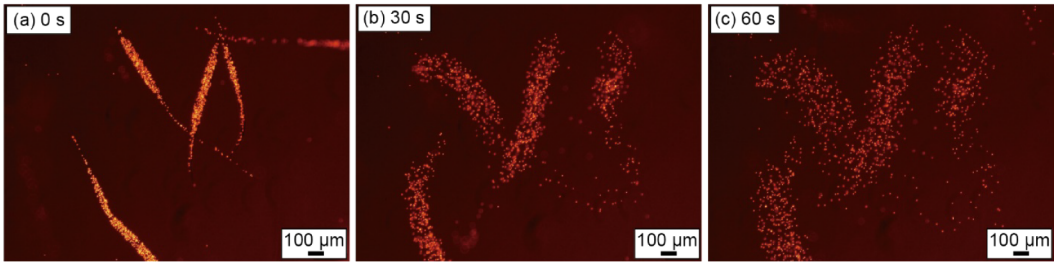

Figure 3. Dissolution of the AF fibers encapsulating red fluorescent particles (φ = 3.2 μm). These microscopic images were captured at (a) 0, (b) 30, and (c) 60 s after dipping the AF fibers in the EDTA solution.

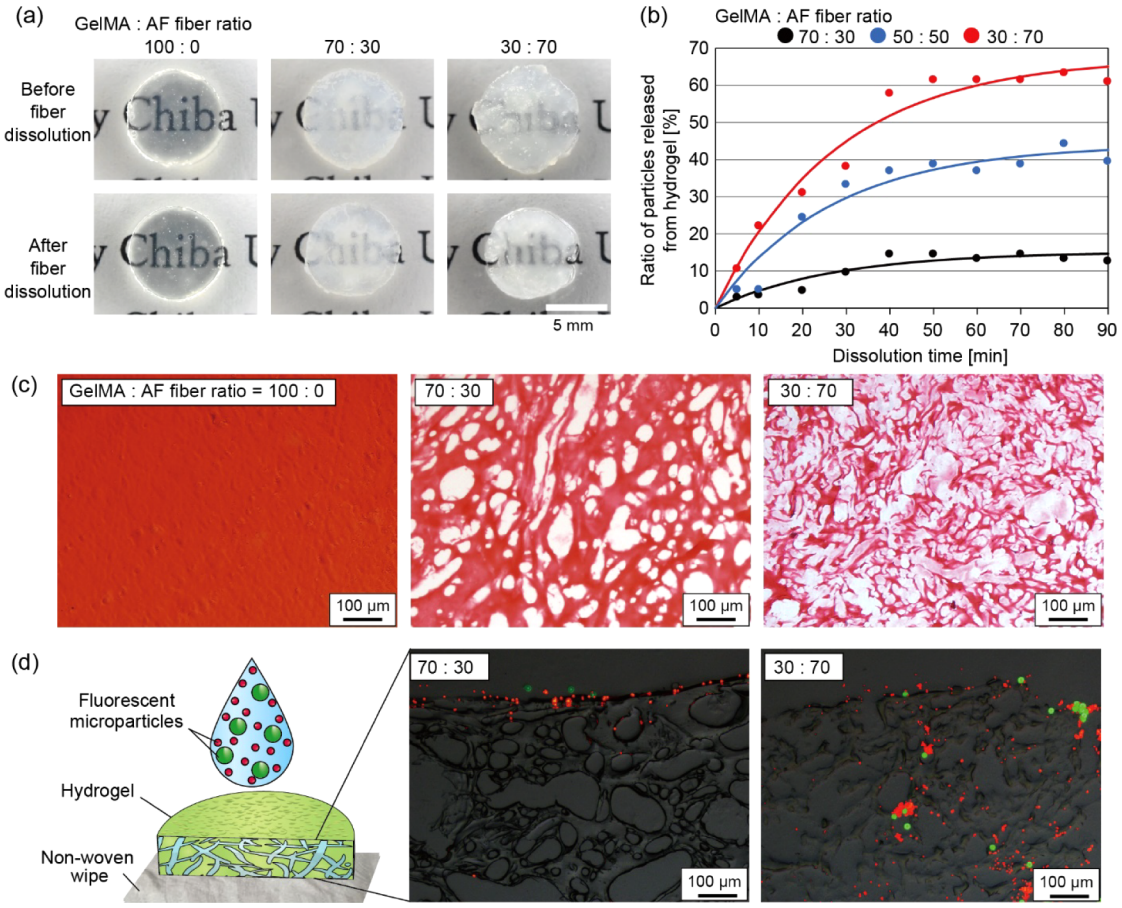

Figure 4. Characterization of the hydrogel sponges. (a) Photographs of the hydrogel before and after dissolving the AF fibers in the EDTA solution. The volume ratio of the GelMA solution and the AF fiber was changed as indicated. (b) The ratios of the particles released from the hydrogel during the dissolution of the AF fibers in the EDTA solution. (c) The cross-sectional morphologies of the uniform hydrogel (100:0 ratio) and hydrogel sponges (70:30 or 30:70 ratio). The GelMA matrices were stained by Picrosirius red. (d) Penetration of fluorescent microparticles dropped onto the hydrogel sponges. Green (9.9 μm) and red (3.2 μm) particles were applied, and the cross sections were directly observed.

nozzle is constant, the thread diameter of the precursor solution extruded from the nozzle is proportional to the square root of the feed flow rate; this tendency was observed in this experiment. The thinnest fibers were 12 μm in the mean diameter and the thickest were 37 μm. AF fibers of such diameter are considered significantly useful for generating high-density conduits that function as capillary networks in hydrogel sponges. The length of the AF fibers increased as the flow rate increased, although the variation in fiber length was relatively large. The increased flow rate of the precursor solution resulted in a smaller difference between the velocities of the extruded and surrounding flows, possibly resulting in a reduced shear force and generation of longer fragments. When PEG with a lower molecular weight (Mw = 6,000) was used as a thickener, the fiber diameter increased by approximately 2-fold (data not shown). This indicates that the viscosity of the gelator solution has a critical impact on the fiber diameter.

The effect of the stirring speed on the fiber morphology was also investigated. As shown in Figure 2c, the effect of the stirring speed on the fiber length was much more significant and the length was changed in a range of 500 to 1500 μm; the higher stirring speed resulted in greater shear force, generating shorter fragments. The AF fibers prepared at 500 rpm were relatively long and easily tangled when dispersed in an aqueous suspension. In the following all experiments AF fibers produced at the stirring speed of 1000 rpm and the flow rate

https://doi.org/10.1021/acsomega.4c08536
ACS Omega 2025, 10, 11900−11910

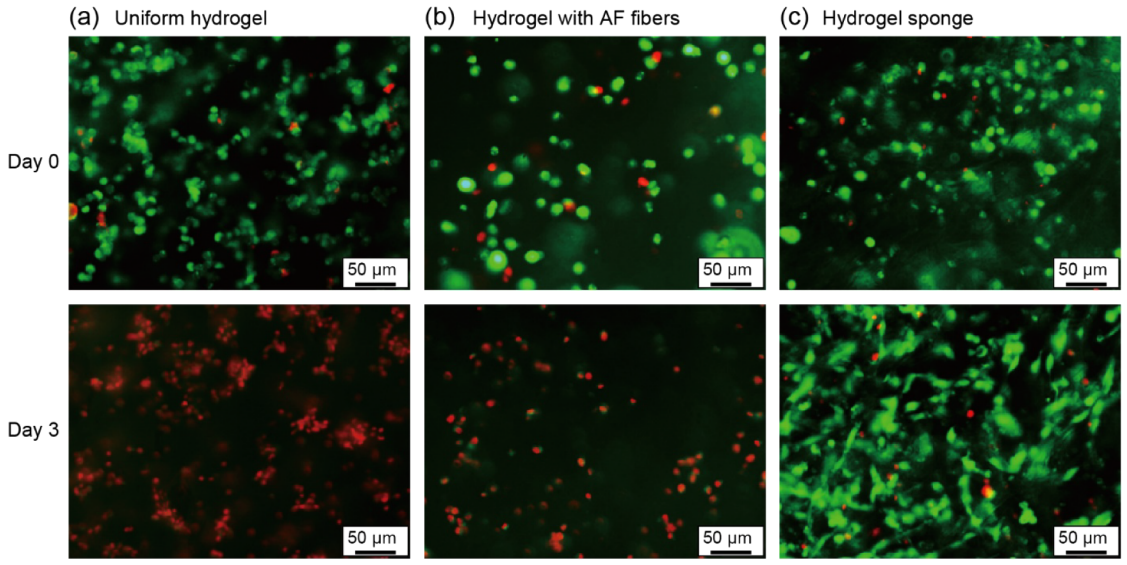

Figure 5. Live/dead assays of the encapsulated HepG2 cells at Days 0 and 3, for (a) uniform hydrogel, (b) hydrogel with embedded AF fibers without the dissolution process, and (c) hydrogel sponge prepared at the volume ratio of the AF fiber of 70%, respectively. Viable cells were stained green and dead cells were stained red.

of 40 μL/min (a mean length of 500 μm and a mean diameter of 16 μm) were used, because longer fibers are more prone to entangling, while thicker fibers risk the leakage of cells from the internal conduits.

3.3. Dissolution of the AF Fibers. The dissolvability of the sacrificial AF fibers is another crucial factor that determines the formation speed and efficiency of hydrogel sponges. Alginate polymers are composed of two types of sugar units, mannuronic acid and guluronic acid, and the stability, strength, and solubility of hydrogels are affected by the ratio of these monomer units to the counter cations.[41,42] In this study, EDTA-3Na was used as the chelating agent for Ca^{2+}, and its concentration was set to 75 mM so that this solution became nearly isotonic. The dissolution behavior of the AF fibers encapsulating 3.2 μm red fluorescent particles was observed. As shown in Figure 3, the fibers immediately began to swell and dissolve when placed in the EDTA solution. After 30 s of incubation, the fibers swelled significantly, and after 60 s, the particles diffused into the surrounding medium. This result clarified that the sacrificial AF fibers can be rapidly removed owing to their high dissolvability and used to form capillary-like conduits in the hydrogel.

3.4. Preparation and Characterization of Hydrogel Sponges. Hydrogel sponges were fabricated using the prepared AF fibers as sacrificial materials. As a hydrogel material for cell encapsulation and cultivation, we chose a photo-cross-linkable gelatin derivative, GelMA, which is often used as a bioink for 3D bioprinter[43,44] and has biocompatible and cell-adhesive properties. Initially, we fabricated hydrogel sponges using cell-free GelMA and the AF fibers. The volume ratio of the AF fibers, which is a crucial parameter for determining the density, morphology, and connectivity of the pores, was varied. The prepared AF fibers were able to be dispersed in a GelMA solution at a high concentration (e.g., the volume ratio of 70%) without entanglement. When the mixed precursor solution with the AF fibers in the chamber was irradiated with UV light, a cylindrical hydrogel plate was formed. Figure 4a shows the photographs of the hydrogels prepared with different volumetric fiber ratios before and after dissolving the fibers. The uniform hydrogels that did not incorporate the AF fibers were relatively transparent. In contrast, as the fiber content increased, the hydrogels became opaque. After treating the hydrogel in the EDTA solution, the hydrogel incorporating the AF fibers at 70% became less opaque, indicating that the fibers were removed by this treatment. To investigate the dissolution behaviors of the AF fibers in detail, we evaluated the ratios of the fluorescent particles released from the AF fibers in the hydrogel to the surrounding medium. As shown in Figure 4b, regardless of the volumetric fiber ratio, the elution of particles reached a plateau after 40 min of dissolution under all conditions. A larger fiber ratio resulted in a higher degree of released particles, indicating that the pores in the hydrogels were more continuous. Notably, when the volume ratio of the AF fibers was 80%, GelMA in the precursor solution was also well cross-linked, but the resulting hydrogel sponge was highly fragile. In addition, 2 mm thick hydrogel sponges were also successfully obtained via UV cross-linking and fiber dissolution.

The density and morphology of the pores inside the hydrogel sponge were then directly observed by preparing thin frozen sections. The hydrogel matrix of GelMA was stained red with Picrosirius red dye. As shown in Figure 4c, no pores were observed in the control hydrogel prepared without fibers. In the hydrogel sponge prepared with 30% of the AF fibers, many pores were formed; however, they seemed mostly independent of each other. The shapes of the pores varied from nearly round to long and thin because the fibers were randomly oriented in the hydrogel. On the other hand, when the volume ratio of the AF fibers was 70%, the pore density became significantly high, and pores were clearly interconnected. Under this condition, the densely arranged pores morphologically mimic capillary networks in some organs, as represented by the sinusoidal capillaries in the liver.[45]

Finally, to further verify whether the internal pores of the hydrogel sponge were sufficiently continuous to transport medium components to deep regions, a particle penetration test was performed. The prepared sponges were placed on a wipe and DI water containing fluorescent particles (3.2 and 9.9

https://doi.org/10.1021/acsomega.4c08536
ACS Omega 2025, 10, 11900−11910

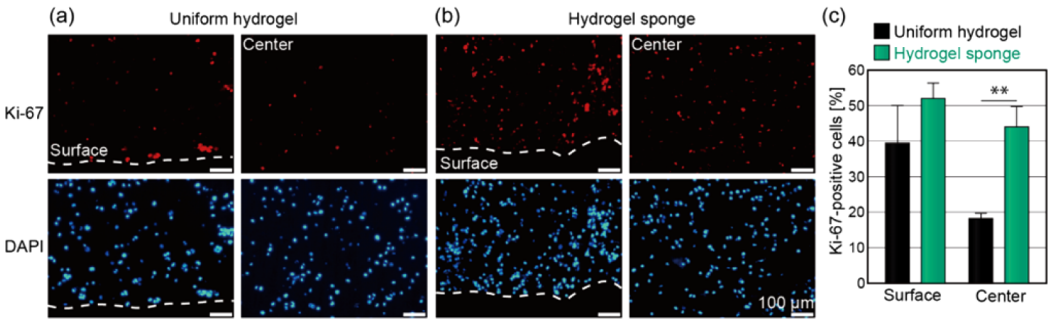

Figure 6. Immunohistochemistry of Ki-67 for HepG2 cells in the (a) uniform hydrogel and (b) hydrogel sponge at Day 3. Dashed white lines indicate the hydrogel surface. (c) Ratios of the Ki-67-positive cells. Each data represents the mean ± SD from 4 samples. $^{**}p < 0.01$.

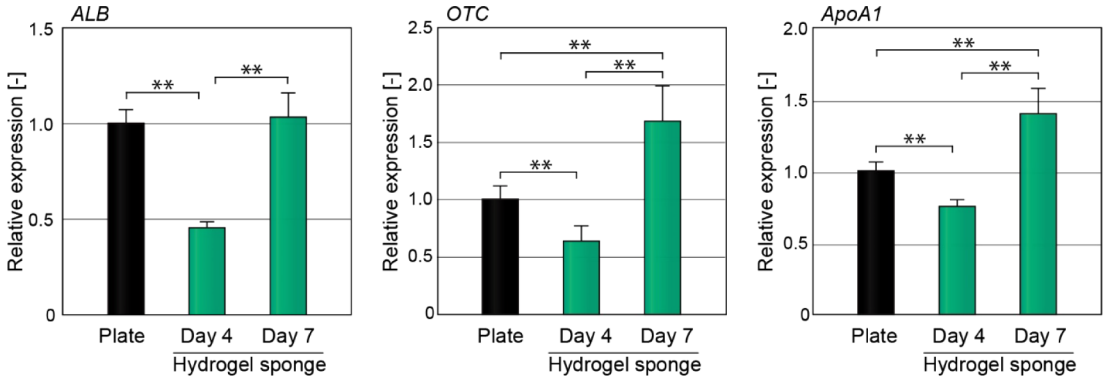

Figure 7. Gene expression analysis of HepG2 cells cultured on a culture plate at Day 3 (70−80% confluency) and encapsulated in the hydrogel sponge (Day 4 and Day 7) by RT-qPCR. *ALB*: albumin; *OTC*: ornithine transcarbamylase; *ApoA1*: apolipoprotein A1. Each data represents the mean ± SD from 6 samples. $^{**}p < 0.01$.

μm) was dropped on top of them, followed by the preparation of frozen sections and microscopic observation. As shown in Figure 4d, in the hydrogel sponge prepared at a volumetric fiber ratio of 30%, the dropped particle suspension remained on the surface, and the particles also did not flow into the sponge. In the hydrogel sponge prepared with 70% fiber, the particle suspension dropped onto the surface and rapidly absorbed through the hydrogel onto a wipe. Cross-sectional observation revealed that the 3.2 μm particles flowed into the inner pores, although the number of the larger 9.9 μm flowed through the matrix was smaller. This result confirmed that the appropriately tailored pores inside the hydrogel sponge were sufficiently continuous to deliver the medium components directly to the hydrogel interior.

3.5. Cultivation of Mammalian Cells in the Matrix of Hydrogel Sponges. As an application of the hydrogel sponges with unique internal microstructures, we created liver tissue models. In the liver, capillary networks are regularly and densely organized. Hepatocytes, the parenchymal cells of the liver, are in close proximity to the capillaries through a thin layer of sinusoidal endothelial cells and are embedded in a matrix containing collagen.[7] We expected that such a cellular arrangement in the hydrogel sponge would mimic the tissue microarchitectures *in vivo* in a sophisticated but highly simplified manner. We used HepG2 cells, a human hepatoma cell line and commonly used as liver cell models with drug metabolism activities.[46,47]

First, we determined whether the presence of cells affected the hydrogel sponge formation. The cell-embedding hydrogel sponges were prepared using a similar process as in the cell-free GelMA hydrogel at a volumetric fiber ratio of 70%. As a result, GelMA was successfully cross-linked and a hydrogel sponge was formed after the dissolution of the AF fibers, even though the density of the cells in the precursor suspension was high (2.5×10^7 cells/mL). This result indicates that sufficient UV light was applied to the precursor suspension, and the presence of the cells did not affect the removal of the sacrificial AF fibers.

To characterize the encapsulated cells, first, cell viability in the GelMA matrix was examined. For this experiment, in addition to the hydrogel sponge, we prepared a uniform hydrogel made of GelMA only as a control and a hydrogel sponge prepared at the fiber ratio of 70% without dissolving the AF fibers. Under these conditions, the concentrations of the cells in the GelMA solution before adding fibers were set to equal, 2.5×10^7 cells/mL. The cell viability in these hydrogels at Days 0 and 3 was evaluated, as shown in Figure 5. At Day 0, more than 90% of the cells were viable in all of these conditions. These results demonstrate that the preparation process of the hydrogel sponge, including the EDTA treatment, did not affect the cell viability. At Day 3, in marked contrast, a significant difference was observed between these conditions. In both the uniform hydrogel and the hydrogel without dissolving the AF fibers, the ratios of viable cells were extremely low, less than 10% (Figure 5a,b). In the hydrogel sponges, the cell viability remained over 90%, and cells exhibited elongated morphologies (Figure 5c). In general, in 3D culture systems using hydrogels, necrosis occurs because of a lack of oxygen supply when the distance from the culture medium increases.[19,20] The results obtained here suggest that in the hydrogel sponges, cell viability was dramatically improved, mostly owing to the positive effect of the

https://doi.org/10.1021/acsomega.4c08536
ACS Omega 2025, 10, 11900−11910

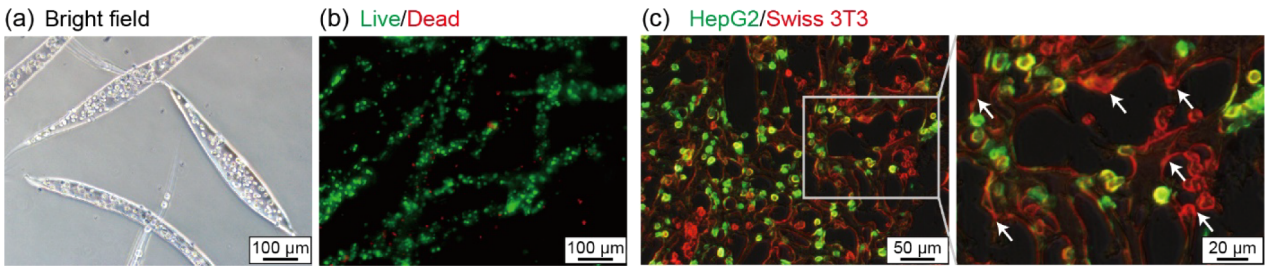

Figure 8. (a) Bright field micrograph of the AF fibers encapsulating Swiss 3T3 cells. (b) Live/dead assay of the Swiss 3T3 cells in the AF fibers. (c) Cross section of the hydrogel sponge encapsulating HepG2 cells (green) in the GelMA hydrogel matrix and Swiss 3T3 cells (red) on the lumen of the inner pores at Day 3. White arrows in the right panel indicate extended 3T3 cells on the lumen.

interconnected internal pores on the enhanced transport of oxygen and nutrients.

The proliferative ability of the encapsulated HepG2 cells was also examined. The expression of the proliferation marker protein Ki-67 was investigated by immunostaining. Comparisons were made with uniform hydrogels prepared without using the AF fibers. In addition, to clarify the positional effects in the hydrogel, we separately observed and evaluated the surface area (within 200 μm from the surface) and the center area (deeper than 200 μm from the surface). The results are shown in Figure 6. In the uniform hydrogel Ki-67 positive cells were present in the surface area; however, those in the center area were limited, only approximately 20% (Figure 6a). In contrast, in the hydrogel sponge, the ratio of Ki-67 positive cells was significantly high both in the surface (52%) and the center (44%) areas (Figure 6b,c). In the hydrogel sponge, HepG2 cells formed small clusters composed of several cells in the hydrogel matrix, even at the center area. This result clarified that the presence of interconnected pores in the hydrogel sponge improved not only cell viability but also cell proliferation.

Finally, the expressions of liver cell-specific genes of HepG2 cells were evaluated using RT-qPCR. It is widely recognized that 3D hepatocyte culture systems are highly beneficial because liver-specific functions are improved.[48] It was speculated that the 3D nature of the hydrogel sponges, along with the support of the vasculature-like conduits, possibly contributed to the enhancement of the functions of the encapsulated cells. We compared the hydrogel sponge with the plate culture as a control. The results are shown in Figure 7. The expression of albumin (*ALB*), one of the representative functions of hepatocytes, was slightly lower in hydrogel sponges at Day 4 than in plate cultures, however, increased by Day 7 and was comparable to that of the plate culture. For ornithine transcarbamylase (*OTC*), a gene involved in urea synthesis, and apolipoprotein A1 (*ApoA1*), a gene involved in lipoprotein synthesis, the expression levels at Day 7 were enhanced compared with those of the plate culture. This result may be attributed to the fact that the cell−cell and/or cell−matrix interaction between proliferated cells became appropriate, and the cells began to express their functions with cell culture proceeded.[49] Although the expression level of albumin at Day 7 was similar to that of the plate culture, it may be further enhanced if the cells are cultured for a longer period of time.[46] These cell characterization experiments demonstrated the benefits of hydrogel sponges and suggested their potential applications in the creation of bioartificial liver devices and liver cell-based drug assays.

3.6. Spatial Positioning of Two Cell Types in the Hydrogel Sponge. Another major advantage of the proposed approach using the sacrificial AF fibers is that the coculture of multiple cell types with controlled spatial positioning can be realized. By placing parenchymal cells inside the GelMA matrix and other cells (e.g., vascular endothelial cells and fibroblasts) in the sacrificial material, different types of cells can be inoculated and cultured simultaneously inside and on the surface of the hydrogel. Here, HepG2 cells inside the GelMA matrix and fibroblasts (3T3 cells) on the lumen of the conduits were cocultured, as 3T3 cells are often used as feeder cells for liver cell cultivation.[50,51]

Before performing the coculture, the impact of encapsulation in the AF fibers on cell viability was investigated. Fibers were prepared from a precursor solution with 2.5×10^7 cells/mL of Swiss 3T3 cells under the condition of 40 μL/min, 1000 rpm. As shown in Figure 8a,b, more than 90% of the cells were viable, suggesting that the gelation and fragmentation process did not substantially affect the cells. It was assumed that once the cells were encapsulated in the alginate hydrogel matrix of the AF fibers, they were less susceptible to the influences of shear force, even under the application of a high shear force during the production of the AF fibers.

Hydrogel sponges were then prepared for coculture. Although the micropores were continuous and they were large to enable the penetration of 9.9 μm particles as described above, the 3T3 cells released from the pore of the hydrogel sponge was less than 10% during the fiber dissolution process. This might be attributed to the relatively large size of the cells (the mean diameter of 13 μm) and their adhesive nature to the surface of the gelatin-based matrix. We then cultured two cell types with controlling their positions. A micrograph showing the cross-section of the hydrogel sponge at Day 3 is shown in Figure 8c, where HepG2 and 3T3 cells were stained green and red, respectively. A cross-sectional micrograph at Day 1 is also shown in Supporting Figure S1. The 3T3 cells exhibited a relatively rounded morphology at Day 1, while some of them had already adhered to the lumen of the internal conduits. At Day 3, 3T3 cells exhibited an elongated morphology on the surface of the hydrogel matrix. Conversely, HepG2 cells were encapsulated in the GelMA matrix and formed relatively rounded small clusters. This difference was attributed to the location of the cells inside or outside the hydrogel, which is similar to the cell positioning found in living tissues.

Current 3D bioprinting techniques are limited in modeling speed and resolution, making it almost impossible to fabricate hydrogel sponges with continuous micropores and simultaneously introduce two cell types into distinct regions. In contrast, our approach achieves high-resolution control of cell

https://doi.org/10.1021/acsomega.4c08536
ACS Omega 2025, 10, 11900−11910

positioning using two types of hydrogels: one removed as a sacrificial porogen and the other functioning as a cell-encapsulating matrix. Owing to the advantages of simplicity in manipulation and high controllability, the proposed method can be applied to the formation of various tissue/organ models in which multiple cell types are densely arranged together with incorporated vasculature-like microconduits.

We have also analyzed the gene expressions of HepG2 cells cocultured with Swiss 3T3 cells in the hydrogel sponge at Day 3 using RT-qPCR. The results are shown in Supporting Figure S2, where the data for the single culture of HepG2 cells in the hydrogel sponge is normalized to 1. The expression of albumin (*ALB*) in the coculture condition was slightly higher than that of the single culture, but the difference was not statistically significant. The difference in ornithine transcarbamylase (*OTC*) expression was also not statistically significant. The lack of observed positive effects of the coculture may be due to insufficient delivery of paracrine signals secreted from 3T3 cells to the embedded HepG2 cells, possibly hindered by the presence of internal conduits. Further optimization of the culture conditions, including the pore density and morphology, is necessary to maximize the effect of coculture on HepG2 cell functions.

4. CONCLUSIONS

We propose a novel approach to realize a hydrogel-based cell culture system that can mimic the complex structure of biological tissues with densely formed microconduits. The first key point is the development of a simple and efficient process of creating AF fibers with desired length/diameter and encapsulating intact cells, which function as a new type of sacrificial porogen. Hydrogel sponges with internal microconduits with a high degree of connectivity can be formed by controlling the morphology and volume ratio of the AF fibers. As we were able to tune the hydrogel morphology and pore density, optimization of the cell culture conditions would be realized to maximize the cell functions and activities.

In this study, GelMA was used as the cell-embedding matrix. However, the proposed approach would be also applicable to other hydrogels. For example, fibrin-based hydrogel sponges will be promising, as fibrin is often used to construct capillary networks of vascular endothelial cells.[52,53] The AF fibers themselves are also highly compatible with 3D bioprinting technology because they are sufficiently dispersible in aqueous precursor solutions for preparing the hydrogels. Owing to the ease of preparation of the AF fibers and their versatility, they are expected to be applicable to various 3D cell culture systems, such as for drug metabolism assays and for elucidating the mechanisms of heterotypic cellular interactions.

■ ASSOCIATED CONTENT

Supporting Information

The Supporting Information is available free of charge at https://pubs.acs.org/doi/10.1021/acsomega.4c08536.

Figures S1: Cross sectional image of the hydrogel sponges for coculture at Days 1 and 3; Figures S2: Gene expression analysis for both single cell culture and coculture with 3T3 cells in hydrogel sponges (PDF)

■ AUTHOR INFORMATION

Corresponding Author

Masumi Yamada − *Department of Applied Chemistry and Biotechnology, Graduate School of Science and Engineering, Chiba University, Chiba 263-8522, Japan;* orcid.org/0000-0003-2596-3527; Email: m-yamada@faculty.chiba-u.jp

Authors

Aruto Hori − *Department of Applied Chemistry and Biotechnology, Graduate School of Science and Engineering, Chiba University, Chiba 263-8522, Japan;* orcid.org/0009-0004-8457-8711

Mizuki Hirata − *Department of Applied Chemistry and Biotechnology, Graduate School of Science and Engineering, Chiba University, Chiba 263-8522, Japan*

Rina Nonogaki − *Department of Applied Chemistry and Biotechnology, Graduate School of Science and Engineering, Chiba University, Chiba 263-8522, Japan*

Rie Utoh − *Department of Applied Chemistry and Biotechnology, Graduate School of Science and Engineering, Chiba University, Chiba 263-8522, Japan*

Complete contact information is available at: https://pubs.acs.org/10.1021/acsomega.4c08536

Author Contributions

The manuscript was written through contributions of all authors. All authors have given approval to the final version of the manuscript.

Notes

The authors declare no competing financial interest.

■ ACKNOWLEDGMENTS

This study was supported in part by Grants-in-Aid for Scientific Research (23K23143 and 20H02529) from the Ministry of Education, Culture, Sports, Science, and Technology of Japan.

■ REFERENCES

(1) Caddeo, S.; Boffito, M.; Sartori, S. Tissue Engineering Approaches in the Design of Healthy and Pathological In Vitro Tissue Models. *Front. Bioeng. Biotechnol.* **2017**, *5*, 40.

(2) Ma, X.; Liu, J.; Zhu, W.; Tang, M.; Lawrence, N.; Yu, C.; Gou, M.; Chen, S. 3D Bioprinting of Functional Tissue Models for Personalized Drug Screening and in Vitro Disease Modeling. *Adv. Drug Delivery Rev.* **2018**, *132*, 235−251.

(3) Axpe, E.; Oyen, M. L. Applications of Alginate-Based Bioinks in 3D Bioprinting. *Int. J. Mol. Sci.* **2016**, *17*, 1976.

(4) Hamedi, E.; Vahedi, N.; Sigaroodi, F.; Parandakh, A.; Hosseinzadeh, S.; Zeinali, F.; Khani, M.-M. Recent Progress of Bioprinted PEGDA-based Bioinks for Tissue Regeneration. *Polym. Adv. Technol.* **2023**, *34*, 3505−3517.

(5) Ghosh, R. N.; Thomas, J.; Vaidehi, B. R.; Devi, N. G.; Janardanan, A.; Namboothiri, P. K.; Peter, M. An Insight into Synthesis, Properties and Applications of Gelatin Methacryloyl Hydrogel for 3D Bioprinting. *Mater. Adv.* **2023**, *4*, 5496−5529.

(6) Su, Z.; Guo, C.; Gui, X.; Wu, L.; Zhang, B.; Qin, Y.; Tan, Z.; Zhou, C.; Wei, W.; Fan, Y.; et al. 3D Printing of Customized Bioceramics for Promoting Bone Tissue Regeneration by Regulating Sympathetic Nerve Behavior. *J. Mater. Chem. B* **2024**, *12*, 4217−4231.

(7) Yamada, M.; Utoh, R.; Ohashi, K.; Tatsumi, K.; Yamato, M.; Okano, T.; Seki, M. Controlled Formation of Heterotypic Hepatic Micro-organoids in Anisotropic Hydrogel Microfibers for Long-term

Preservation of Liver-specific Functions. *Biomaterials* **2012**, *33*, 8304−8315.
(8) Liu, X.; Wang, X.; Zhang, L.; Sun, L.; Wang, H.; Zhao, H.; Zhang, Z.; Liu, W.; Huang, Y.; Ji, S. 3D Liver Tissue Model with Branched Vascular Networks by Multimaterial Bioprinting. *Adv. Healthcare Mater.* **2021**, *10*, No. e2101405.
(9) Khati, V.; Turkki, J. A.; Ramachandraiah, H.; Pati, F.; Gaudenzi, G.; Russom, A. Indirect 3D Bioprinting of a Robust Trilobular Hepatic Construct with Decellularized Liver Matrix Hydrogel. *Bioengineering* **2022**, *9*, 603.
(10) Thomas, A.; Orellano, I.; Lam, T.; Noichl, B.; Geiger, M.-A.; Amler, A.-K.; Kreuder, A.-E.; Palmer, C.; Duda, G.; Lauster, R.; et al. Vascular Bioprinting with Enzymatically Degradable Bioinks via Multi-material Projection-based Stereolithography. *Acta Biomater.* **2020**, *117*, 121−132.
(11) Martinez-Moreno, D.; Venegas-Bustos, D.; Rus, G.; Galvez-Martin, P.; Jimenez, G.; Marchal, J. A. Chondro-Inductive b-TPUe-Based Functionalized Scaffolds for Application in Cartilage Tissue Engineering. *Adv. Healthcare Mater.* **2022**, *11*, No. e2200251.
(12) Kim, S.; Choi, C.; Cha, C. Mechanotopography-Driven Design of Dispersible Nanofiber-Laden Hydrogel as a 3D Cell Culture Platform for Investigating Tissue Fibrosis. *Adv. Healthcare Mater.* **2021**, *10*, No. e2101109.
(13) Murphy, C. A.; Lim, K. S.; Woodfield, T. B. F. Next Evolution in Organ-Scale Biofabrication: Bioresin Design for Rapid High-Resolution Vat Polymerization. *Adv. Mater.* **2022**, *34*, No. e2107759.
(14) Liu, X.; Ren, Y.; Fu, S.; Chen, X.; Hu, M.; Wang, F.; Wang, L.; Li, C. Toward Morphologically Relevant Extracellular Matrix: Nanofiber-hydrogel Composites for Tumor Cell Culture. *J. Mater. Chem. B* **2024**, *12*, 3984−3995.
(15) Levenberg, S.; Rouwkema, J.; Macdonald, M.; Garfein, E. S.; Kohane, D. S.; Darland, D. C.; Marini, R.; van Blitterswijk, C. A.; Mulligan, R. C.; D'Amore, P. A.; et al. Engineering Vascularized Skeletal Muscle Tissue. *Nat. Biotechnol.* **2005**, *23*, 879−884.
(16) Anada, T.; Fukuda, J.; Sai, Y.; Suzuki, O. An Oxygen-permeable Spheroid Culture System for the Prevention of Central Hypoxia and Necrosis of Spheroids. *Biomaterials* **2012**, *33*, 8430−8441.
(17) Ichihara, Y.; Utoh, R.; Yamada, M.; Shimizu, T.; Uchigata, Y. Size Effect of Engineered Islets Prepared Using Microfabricated Wells on Islet Cell Function and Arrangement. *Heliyon* **2016**, *2*, No. e00129.
(18) Murphy, A. R.; Allenby, M. C. In Vitro Microvascular Engineering Approaches and Strategies for Interstitial Tissue Integration. *Acta Biomater.* **2023**, *171*, 114−130.
(19) Szot, C. S.; Buchanan, C. F.; Freeman, J. W.; Rylander, M. N. 3D in Vitro Bioengineered Tumors Based on Collagen I Hydrogels. *Biomaterials* **2011**, *32*, 7905−7912.
(20) Ishida-Ishihara, S.; Takada, R.; Furusawa, K.; Ishihara, S.; Haga, H. Improvement of The Cell Viability of Hepatocytes Cultured in Three-dimensional Collagen Gels Using Pump-free Perfusion Driven by Water Level Difference. *Sci. Rep.* **2022**, *12*, 20269.
(21) Liu, S.; Wang, T.; Li, S.; Wang, X. Application Status of Sacrificial Biomaterials in 3D Bioprinting. *Polymers* **2022**, *14*, 2182.
(22) Li, S.; Li, H.; Shang, X.; He, J.; Hu, Y. Recent Advances in 3D Printing Sacrificial Templates for Fabricating Engineered Vasculature. *MedComm: Biomater. Appl.* **2023**, *2*, No. e46.
(23) Kolesky, D. B.; Truby, R. L.; Gladman, A. S.; Busbee, T. A.; Homan, K. A.; Lewis, J. A. 3D Bioprinting of Vascularized, Heterogeneous Cell-laden Tissue Constructs. *Adv. Mater.* **2014**, *26*, 3124−3130.
(24) Contessi Negrini, N.; Bonnetier, M.; Giatsidis, G.; Orgill, D. P.; Fare, S.; Marelli, B. Tissue-mimicking Gelatin Scaffolds by Alginate Sacrificial Templates for Adipose Tissue Engineering. *Acta Biomater.* **2019**, *87*, 61−75.
(25) Matsunaga, Y. T.; Morimoto, Y.; Takeuchi, S. Molding Cell Beads for Rapid Construction of Macroscopic 3D Tissue Architecture. *Adv. Mater.* **2011**, *23*, H90−H94.
(26) Yajima, Y.; Yamada, M.; Utoh, R.; Seki, M. Collagen Microparticle-Mediated 3D Cell Organization: A Facile Route to Bottom-up Engineering of Thick and Porous Tissues. *ACS Biomater. Sci. Eng.* **2017**, *3*, 2144−2154.
(27) Morita, A.; Yamada, M.; Utoh, R.; Momiyama, K.; Iwadate, H.; Seki, M. Formation of 3D Tissues of Primary Hepatocytes Using Fibrillized Collagen Microparticles as Intercellular Binders. *J. Biosci. Bioeng.* **2022**, *133*, 265−272.
(28) Hori, A.; Watabe, Y.; Yamada, M.; Yajima, Y.; Utoh, R.; Seki, M. One-Step Formation of Microporous Hydrogel Sponges Encapsulating Living Cells by Utilizing Bicontinuous Dispersion of Aqueous Polymer Solutions. *ACS Appl. Bio Mater.* **2019**, *2*, 2237−2245.
(29) Yi, S.; Liu, Q.; Luo, Z.; He, J. J.; Ma, H. L.; Li, W.; Wang, D.; Zhou, C.; Garciamendez, C. E.; Hou, L. Micropore-Forming Gelatin Methacryloyl (GelMA) Bioink Toolbox 2.0: Designable Tunability and Adaptability for 3D Bioprinting Applications. *Small* **2022**, *18*, No. e2106357.
(30) Ben Messaoud, G.; Aveic, S.; Wachendoerfer, M.; Fischer, H.; Richtering, W. 3D Printable Gelatin Methacryloyl (GelMA)-Dextran Aqueous Two-Phase System with Tunable Pores Structure and Size Enables Physiological Behavior of Embedded Cells In Vitro. *Small* **2023**, *19*, No. e2208089.
(31) Pan, B.; Shao, L.; Jiang, J.; Zou, S.; Kong, H.; Hou, R.; Yao, Y.; Du, J.; Jin, Y. 3D printing Sacrificial Templates for Manufacturing Hydrogel Constructs with Channel Networks. *Mater. Des.* **2022**, *222*, 111012.
(32) Cheng, K. C.; Theato, P.; Hsu, S. H. 3D-bioprintable Endothelial Cell-laden Sacrificial Ink for Fabrication of Microvessel Networks. *Biofabrication* **2023**, *15*, 045026.
(33) Seymour, A. J.; Kilian, D.; Navarro, R. S.; Hull, S. M.; Heilshorn, S. C. 3D Printing Microporous Scaffolds from Modular Bioinks Containing Sacrificial, Cell-encapsulating Microgels. *Biomater. Sci.* **2023**, *11*, 7598−7615.
(34) Sugimoto, M.; Kitagawa, Y.; Yamada, M.; Yajima, Y.; Utoh, R.; Seki, M. Micropassage-embedding Composite Hydrogel Fibers Enable Quantitative Evaluation of Cancer Cell Invasion under 3D Coculture Conditions. *Lab Chip* **2018**, *18*, 1378−1387.
(35) Utoh, R.; Enomoto, S.; Yamada, M.; Yamanaka, K.; Yajima, Y.; Furusawa, K.; Seki, M. Polyanion-induced, Microfluidic Engineering of Fragmented Collagen Microfibers for Reconstituting Extracellular Environments of 3D Hepatocyte Culture. *Mater. Sci. Eng., C* **2021**, *129*, 112417.
(36) Occhetta, P.; Visone, R.; Russo, L.; Cipolla, L.; Moretti, M.; Rasponi, M. VA-086 Methacrylate Gelatine Photopolymerizable Hydrogels: A Parametric Study for Highly Biocompatible 3D Cell Embedding. *J. Biomed. Mater. Res., Part A* **2015**, *103*, 2109−2117.
(37) Saeki, K.; Hiramatsu, H.; Hori, A.; Hirai, Y.; Yamada, M.; Utoh, R.; Seki, M. Sacrificial Alginate-Assisted Microfluidic Engineering of Cell-Supportive Protein Microfibers for Hydrogel-Based Cell Encapsulation. *ACS Omega* **2020**, *5*, 21641−21650.
(38) Kato-Negishi, M.; Sawayama, J.; Kawahara, M.; Takeuchi, S. Cell Fiber-based 3D Tissue Array for Drug Response Assay. *Sci. Rep.* **2022**, *12*, 7870.
(39) Martino, C.; Statzer, C.; Vigolo, D.; deMello, A. J. Controllable Generation and Encapsulation of Alginate Fibers Using Droplet-based Microfluidics. *Lab Chip* **2016**, *16*, 59−64.
(40) Deng, X.; Ren, Y.; Hou, L.; Liu, W.; Jia, Y.; Jiang, H. Electric Field-Induced Cutting of Hydrogel Microfibers with Precise Length Control for Micromotors and Building Blocks. *ACS Appl. Mater. Interfaces* **2018**, *10*, 40228−40237.
(41) Morch, Ý. A.; Donati, I.; Strand, B. L.; Skjak-Braek, G. Effect of Ca^{2+}, Ba^{2+}, and Sr^{2+} on Alginate Microbeads. *Biomacromolecules* **2006**, *7*, 1471−1480.
(42) Draget, K. I.; Skjåk-Bræk, G.; Stokke, B. T. Similarities and Differences between Alginic Acid Gels and Ionically Crosslinked Alginate Gels. *Food Hydrocolloids* **2006**, *20*, 170−175.
(43) Hwangbo, H.; Lee, H.; Jin, E.-J.; Lee, J.; Jo, Y.; Ryu, D.; Kim, G. Bio-printing of Aligned GelMa-based Cell-laden Structure for Muscle Tissue Regeneration. *Bioact. Mater.* **2022**, *8*, 57−70.

https://doi.org/10.1021/acsomega.4c08536
ACS Omega 2025, 10, 11900−11910

(44) Guo, A.; Zhang, S.; Yang, R.; Sui, C. Enhancing The Mechanical Strength of 3D Printed GelMA for Soft Tissue Engineering Applications. *Mater. Today Bio* **2024**, *24*, 100939.
(45) Utoh, R.; Komori, J.; Kuge, H.; Tatsumi, K.; Yamada, M.; Hirohashi, S.; Tsutsumi, M.; Amanuma, T.; Yoshioka, A.; Nakajima, Y.; et al. Adult Hepatocytes Direct Liver Organogenesis through Non-parenchymal Cell Recruitment in The Kidney. *J. Hepatol.* **2018**, *68*, 744−753.
(46) Ramaiahgari, S. C.; den Braver, M. W.; Herpers, B.; Terpstra, V.; Commandeur, J. N. M.; van de Water, B.; Price, L. S. A 3D in Vitro Model of Differentiated HepG2 Cell Spheroids with Improved Liver-like Properties for Repeated Dose High-throughput Toxicity Studies. *Arch. Toxicol.* **2014**, *88*, 1083−1095.
(47) Arzumanian, V. A.; Kiseleva, O. I.; Poverennaya, E. V. The Curious Case of the HepG2 Cell Line: 40 Years of Expertise. *Int. J. Mol. Sci.* **2021**, *22*, 13135.
(48) Yoon No, D.; Lee, K.-H.; Lee, J.; Lee, S.-H. 3D Liver Models on a Microplatform: Well-Defined Culture, Engineering of Liver Tissue and Liver-on-a-chip. *Lab Chip* **2015**, *15*, 3822−3837.
(49) Yamada, M.; Hori, A.; Sugaya, S.; Yajima, Y.; Utoh, R.; Yamato, M.; Seki, M. Cell-sized Condensed Collagen Microparticles for Preparing Microengineered Composite Spheroids of Primary Hepatocytes. *Lab Chip* **2015**, *15*, 3941−3951.
(50) Kobayashi, A.; Yamakoshi, K.; Yajima, Y.; Utoh, R.; Yamada, M.; Seki, M. Preparation of Stripe-patterned Heterogeneous Hydrogel Sheets Using Microfluidic Devices for High-density Coculture of Hepatocytes and Fibroblasts. *J. Biosci. Bioeng.* **2013**, *116*, 761−767.
(51) March, S.; Ramanan, V.; Trehan, K.; Ng, S.; Galstian, A.; Gural, N.; Scull, M. A.; Shlomai, A.; Mota, M. M.; Fleming, H. E.; et al. Micropatterned Coculture of Primary Human Hepatocytes and Supportive Cells for The Study of Hepatotropic Pathogens. *Nat. Protoc.* **2015**, *10*, 2027−2053.
(52) Yeon, J. H.; Ryu, H. R.; Chung, M.; Hu, Q. P.; Jeon, N. L. In Vitro Formation and Characterization of a Perfusable Three-dimensional Tubular Capillary Network in Microfluidic Devices. *Lab Chip* **2012**, *12*, 2815−2822.
(53) Moya, M. L.; Hsu, Y.-H.; Lee, A. P.; Hughes, C. C. W.; George, S. C. In Vitro Perfused Human Capillary Networks. *Tissue Eng., Part C* **2013**, *19*, 730−737.

https://doi.org/10.1021/acsomega.4c08536
ACS Omega 2025, 10, 11900−11910